Tikrit Journal of Engineering Sciences (2023) 30 (3): 27-37
DOI: http://doi.org/10.25130/tjes.30.3.4

IRAQI Academic Scientific Journals

ISSN: 1813-162X (Print); 2312-7589 (Online)
Tikrit Journal of Engineering Sciences
available online at: http://www.tj-es.com

TJES Tikrit Journal of Engineering Sciences

Closed Solar Air Heater System Integrated with PCM (RT42 and RT50) in a Thermal Storage-Finned Heat Exchanger Unit

Hussam S. Dheyab [a,b], Manar S.M. Al-Jethelah [b *], Thamir K. Ibrahim [b], Sirine Chtourou [a], Mounir Baccar [a]

a Laboratory Advanced Fluid Dynamics Energetic and Environment, National School of Engineers of Sfax (ENIS), University of Sfax, 3038, Tunisia.
b Mechanical Engineering Department, College of Engineering, Tikrit University, Iraq.

Keywords:
Solar Air Heater; Phase Change Material; Finned Heat Exchanger; Stored Energy; Recovered Energy.

ARTICLE INFO

Article history:

Received	15 Apr.	2023
Received in revised form	29 Apr.	2023
Accepted	20 June	2023
Final Proofreading	28 July	2023
Available online	01 Sep.	2023

Citation: Dheyab HS, Al-Jethelah MSM, Ibrahim TK, Chtourou S, Baccar M. **Closed Solar Air Heater System Integrated with PCM (RT42 and RT 50) in a Thermal Storage-Finned Heat Exchanger Unit**. *Tikrit Journal of Engineering Sciences* 2023; **30**(3): 27-37.
http://doi.org/10.25130/tjes.30.3.4

*Corresponding author:
Manar S.M. Al-Jethelah
Mechanical Engineering Department, College of Engineering, Tikrit University, Iraq.

Abstract: Utilizing thermal storage integrated into a solar air heater SAH is a promising solution to enhance the thermal performance of solar air heaters. The present work experimentally investigated the thermal impact of an absorber-finned heat exchanger-thermal storage unit integrated inside a solar air heater. The experiments were conducted under the conditions of Tikrit-Iraq in December 2021 and January 2022. RT42 and RT50 were used as PCMs in two separate solar air heaters. Each PCM filled the thermal storage of SAH. A finned heat exchanger, in which air was forced through, was immersed in the thermal storage. Two arrangements were tested. In the first arrangement, the two SAHs were separated from each other. In the second arrangement, the two SAHs were connected in series, first the RT42 SAH and then the RT50 SAH. The results showed that the highest recorded temperature was for RT50, i.e., 59 °C, in the separation arrangement. Also, the solar air heater with RT50 in the series arrangement continued to heat the forced air until 5 AM the next day.

منظومة سخان هواء شمسي مغلقة متكاملة مع مادة متغيرة الطور (RT42 و RT 50) في وحدة خزان حراري-مبادل حراري مزعنف

حسام سامي ذياب [1،2]، منار صالح مهدي الجذلة[2]، ثامر خليل ابراهيم [2]، سيرين شطورو[1]، منير بكار[1]
[1] المختبر المتقدم ديناميكيات السوائل النشطة والبيئة / المدرسة الوطنية لمهندسي صفاقس / جامعة صفاقس/ تونس.
[2] قسم الهندسة المكانيكية / كلية الهندسة / جامعة تكريت / تكريت - العراق.

الخلاصة

إن استعمال خزان حراري متكامل في سخان هواء شمسي يعد حلًا واعدًا لتحسين الأداء الحراري لسخانات الهواء الشمسية. في البحث الحالي تم اجراء دراسة عملية للتأثير الحراري لوحدة ماص-مبادل حراري مزعنف-خزان حراري داخل سخان هواء شمسي. تم اجراء التجارب وفق الظروف الجوية لمدينة تكريت- العراق في كانون الأول 2021 وكانون الثاني 2022. تم استعمال RT42 وRT50 كمواد متغيرة الطور داخل سخاني هواء شمسيين منفصلين. كل مادة متغيرة الطور ملأت الخزان الحراري سخان هواء شمسي. تم غمر مبادل حراري مزعنف- حيث يجبر الهواء عبره- في الخزان الحراري. تم دراسة ترتيبين. في الترتيب الأول كان سخاني الهواء الشمسيين منفصلين عن بعضهما البعض. وفي الترتيب الثاني رُبط سخاني الهواء الشمسيين على التوالي، بحيث كان سخان الهواء الشمسي الحاوي RT42 الأول والحاوي RT50 كان الثاني من حيث الترتيب. بينت النتائج أن أعلى درجة حرارة مسجلة كانت 59 °C لـRT50 في الترتيب المنفصل. كما أن سخان الهواء الشمسي الحاوي RT50 في الترتيب المتوالي استمر في تسخين الهواء المار خلاله حتى الساعة 5 صباحًا لليوم التالي.

الكلمات الدالة: سخان هواء شمسي، مادة متغيرة الطور، مبادل حراري مزعنف، طاقة مخزونة، طاقة مستعادة، كفاءة.

1.INTRODUCTION

Fossil fuel has been associated with various issues as global warming, repeated energy crises, and price fluctuation [1,2]. Solar energy has received outstanding academic and industrial interest in an attempt to reduce global warming and overcome fossil fuel drawbacks [3,4]. One of the most practical and widespread solar energy systems is the solar air heater (SAH). The reliability of SAHs encourages using them in many domestic, industrial, and agricultural applications [5,6]. The SAHs' components have been under investigation to produce more efficient heaters. Like all other solar energy applications, the absence of solar radiation on nights and cloudy days represents a considerable drawback in the solar energy field. Latent heat storage has a crucial benefit in terms of expanding the thermal solar energy applications work [7,8]. Therefore, numerous researchers investigated the possible thermal enhancement gained using phase change materials (PCMs) as thermal storage [9,10]. Wang et al. [11] investigated experimentally the solar air heater SAH thermal performance constructed from flat micro-heat pipe arrays filled with lauric acid ($T_{m,av}$ = 43°C). The results showed that the charging and discharging rates are positively proportional to the air volume flow rate. At 240 m^3/h, the PCM melted within 134 min and solidified within 153 min. Besides, Saxena et al. [12] studied experimentally and compared a reference SAH without PCM to another modified SAH filled with PCM, i.e., paraffin wax ($T_{m,av}$= 42 °C). They found that the thermal efficiency and the heat transfer coefficient of the modified solar air heater were 7.41% and 139.81 W/m^2 K, respectively, higher than the conventional solar system SAH. Furthermore, the SAHs with flat/ v-corrugated absorber plates were experimentally studied by Kabeel et al. [13]. The analyzed SAHs were integrated with thermal storage, i.e., paraffin wax, located under the absorber plate. The authors found that using the phase change material enhanced the air heater's daily efficiency by 12% compared with the case without PCM. El Khadraoui et al. [14] experimentally investigated the effect of integrating paraffin wax ($T_{m,av}$= 56-60 °C) in a solar dryer. The results revealed that the drying chamber remained all night at 4-16 °C above the ambient temperature. Investigating the impact of reflectors on thermal solar applications has also attracted attention. Bhowmik and Amin [15] found an enhancement of 10% in the solar collector efficiency using a reflector. Although using thermal storage filled with a PCM positively impacts SAH, the phase change materials suffer from low thermal conductivity [16–18]. This issue inspired researchers to study possible solutions to enhance thermal storage performance [19–21]. Sajawal et al. [22] experimentally studied the thermal performance of three double-pass solar air heaters. The first one was without PCM. In the second one, semicircular finned pipes filled with RT44 were placed in the upper pass of the heater. In the third configuration, the RT44 was maintained in the upper pass. while the circular finned pipes were filled with RT18 and placed in the heater's lower pass. The results showed that the thermal efficiencies for the first, second, and third configurations were enhanced by 53.2%, 68.4%, and 71.9%, respectively. In addition, Abuşka et al. [23] experimentally examined three flat plate solar air heater configurations. The first one was integrated RT54HC with a honeycomb structure. In the second configuration, only RT54HC was studied. In the third configuration, a conventional SAH, i.e., without PCM nor honeycomb, was studied for comparison. The authors discovered that with

the RT54HC- honeycomb configuration, the charging and discharging periods were reduced. Also, it was found that the configurations with RT54HC showed higher daily thermal efficiency enhancement from 2.6% to 22.3%. Dheyab et al. [24] proposed a novel collector-type solar air heater design. The proposed design was an internal storage of a SAH system filled with PCM integrated with a finned heat exchanger. The experiments were conducted in the summer. The studied solar collector's thermal performance was investigated under 0.25, 0.045, and 0.065kg/s. The studied PCMs were RT42 and RT50. It was found that the charging and discharging efficiencies were enhanced by 90.7% and 93.3%, respectively, using RT42, while using RT50 by 87% and 88.1%, respectively. The present work investigates the thermal performance of a new SAH system design during winter (December 2021 and January 2022). The new design is a closed SAH system that includes an internal thermal storage-finned heat exchanger unit. The proposed technique has yet to be investigated by other researchers, as far as the authors know. The work aims to enhance the SAH by using a PCM. Since the PCMs' thermal conductivities are low, a finned heat exchanger was immersed in the SAH's thermal storage. To reduce heat losses, the thermal storage-finned heat exchanger unit was fixed inside the studied SAHs. The thermal storage-finned heat exchanger unit was heated from above by solar insolation (direct heating) and from below by circulating air inside the air heater around the unit (indirect heating). For an air mass flow rate of 0.065 kg/s, the charging and discharging efficiencies were studied for both separation and series arrangements with RT42 and RT50.

2.EXPERIMENTAL METHODOLOGY

The present work investigated the impact of latent thermal storage on a SAH's thermal performance. The experiments were conducted under the conditions of Tikrit- Iraq (34.67° N, 43.65° E). The tests were conducted in winter from December 2021 to January 2022. The following subsections present the experimental apparatus, data processing, and uncertainty.

2.1.Experimental Set-Up

The experimental set-up included two-identical SAHs, as shown in Fig. 1. Each SAH consisted of a flat absorber (65 cm×65 cm), a glass cover (99 cm ×64 cm, 4mm-thickness, reflectivity =8%, and transmissivity =95%[25,26]), and thermal storage-finned-heat exchanger unit located in the SAH's, Fig. 2. Each heater included a finned heat exchanger (100 cm-long, 65 cm-width, 12 cm-height). The 80 heat exchanger pipes were finned and made from copper (11.8 mm ID and 12.7 mm OD), Fig. 3. The thermal storage-finned-heat exchanger unit's upper surface represented an absorber of the SAH. A channel was constructed to allow air circulation around the thermal storage-finned heat exchanger unit, as shown in Fig. 3. The heat exchanger was immersed in 50 kg of Rubitherm PCM inside thermal storage. The solar collector was covered from its sides and below with a wool glass thermal insulator (2 cm thickness) to maintain the heat inside the air heater and reduce its heat losses. In order to reflect extra solar radiation on the absorber, a 100 cm-long, 65 cm-width- mirror was pivoted above the solar collector glass cover. RT42 filled the thermal storage of the first heater, and RT50 filled the second heater's thermal storage. The RT42 and RT50 thermophysical properties are tabulated in Table 1 [27]. The effect of the gradual heating of the air, which was forced through the heat exchanger, during the discharging period was studied by connecting the two SAHs in series to identify the system's performance compared to the separation arrangement of each SAH, as described in Fig. 4. 12 K-type thermocouples were used to measure the temperatures of the studied PCMs, ambient, and outlet air. Besides, the air velocity, i.e., during discharging, and the wind were measured by a turbine anemometer. In addition, a solar power meter, SM206, was used to measure the solar radiation. The range and accuracy of used measurement devices are tabulated in Table 2.

Table 1 The RT42 and RT50 Thermo-Physical Properties [27]

Properties	RT42		TR50	
T_m	38-43°C		45-51°C	
h_f	165 kJ/kg		160 kJ/kg	
k	0.2 W/m.K		0.2 W/m.K	
c_p	2 kJ/kg K		2 kJ/kg K	
ρ	Solid	Liquid	Solid	Liquid
	0.88 kg/l	0.76 kg/l	0.88 kg/l	0.76 kg/l

Table 2 Range and Accuracy of Used Measurement Devices

Parameter	Measurement Device	Range	Accuracy
Temperature	Thermocouple	-50°C to 100°C	±2.2 °C or 0.75%
Air Velocity	Turbine Anemometer	0.0- 45.0 m/s	± 0.1 m/s or ± 3%
Solar Radiation	Solar Power Meter, SM206	0.1-1999.9W/m²	±10 W/m²

Fig. 1 The Experimental Apparatus.

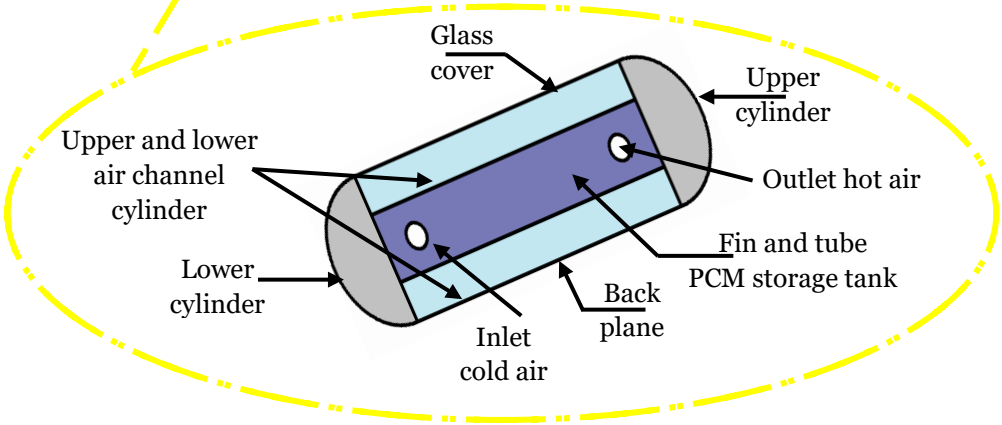

Fig. 2 Closed Solar Air Heater with Internal Thermal Storage Unit.

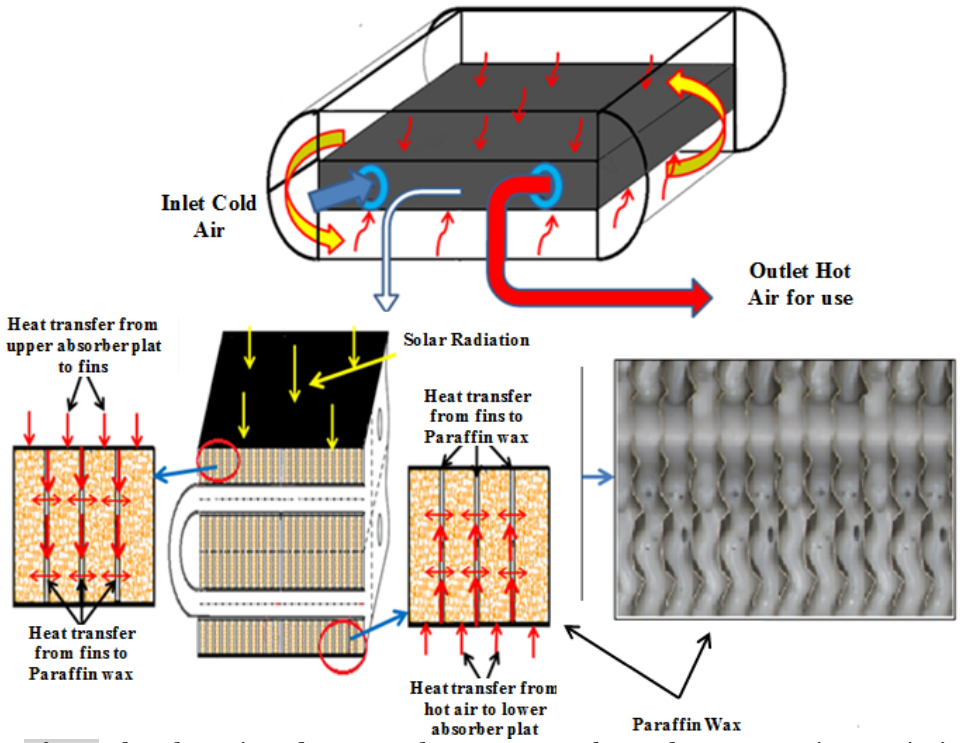

Fig. 3 Absorber-Finned Heat Exchanger-PCM Thermal Storage Unit Description.

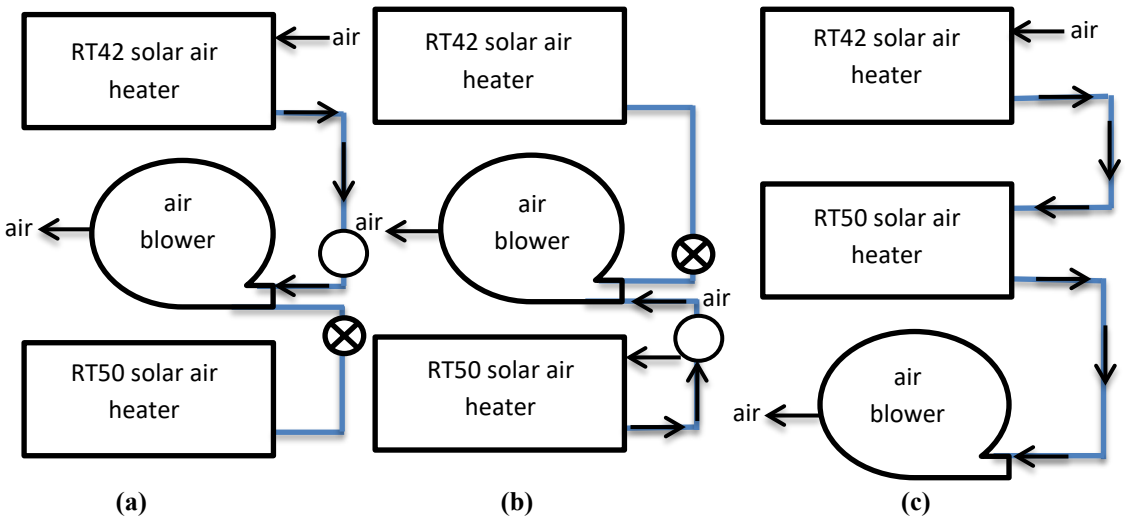

Fig. 4 Schematic of the Arrangements (a) RT42- Separation, (b) RT50- Separation, (c) Series.

2.2.Data Processing

The SAHs' thermal performance was investigated based on the stored and discharged thermal powers and the charging and discharging efficiencies. The SAH's thermal energy balance can be expressed as [5-6]:

$$P_{abs} = P_{storage} + P_{losses} \quad (1)$$

$$P_{abs} = \alpha\, \tau\, \bar{I}\, A \quad (2)$$

where P_{abs} is the total absorbed power by the absorber plate surface, $P_{storage}$ is stored power, P_{losses} is total thermal losses, $\bar{I}$ is the average incident solar energy during the charging period, and A is the aperture area. The amount of power stored during charging and recovered for discharging period inside the storage unit is expressed as [28],

$$P_{stored} = M_{PCM}\left[C_{P,S}(T_m - T_{int}) + h_f + C_{P,l}(T_{fin} - T_m)\right]/\Delta t_{ch} \quad (3)$$

$$P_{recovered} = M_{PCM}\left[C_{P,l}(T_m - T_{fin-dis}) + h_f + C_{P,s}(T_{int-dis} - T_m)\right] /\Delta t_{dis} \quad (4)$$

where M_{PCM} is the mass of PCM, $C_{P,S}$ and $C_{P,l}$. are the specific heat of the PCM in the solid and liquid phase, t is the increment in time, T_{int} and T_{fin} are the initial and final temperature of the PCM, h_f is the latent heat of the PCM, and T_m is the melting temperature of the PCM. The general equation of losses power from the external surfaces of each solar air heater SAH part is defined as,

$$P_{loss\,,\ total} = [P_{g.c} + P_{b.p} + P_{a-ch} + P_{s.s.t} + P_{c.e}] \quad (5)$$

The charging efficiency (η_{charg}) and discharging efficiency ($\eta_{discharg}$) can be written as [29,30],

$$\eta_{charg} = \frac{P_{storage}}{P_{abs}} \quad (6)$$

$$\eta_{discharg} = \frac{P_{used}}{P_{storage}} \quad (7)$$

where P_{used} is the used power that can be defined as [31],

$$P_{used} = \dot{m}\, c_p\, (T_o - T_i) \quad (8)$$

2.3.The Uncertainty

Calculating uncertainties in any experimental investigation is crucial to consider unavoidable errors in measurement devices. The present experimental work measured data are the temperatures of PCMs, the absorber surfaces, the plate at the bottom of the SAH, the glass, and the ambient; air velocity; and solar radiation. The uncertainty calculations in the present investigation followed the Kline and McClintock method [32]. The fractional uncertainty for the absorbed power is

$$\frac{w_{Q_{abs}}}{Q_{abs}} = \frac{w_I}{I} \quad (9)$$

The fractional uncertainty for the useful power is

$$\frac{w_{Q_{use}}}{Q_{use}} = \left[\left(\frac{w_{\dot{m}}}{\dot{m}}\right)^2 + \left(\frac{w_T}{T}\right)^2\right]^{1/2} \quad (10)$$

The fractional uncertainty for the stored power is

$$\frac{w_{Q_{str}}}{Q_{str}} = \frac{w_T}{T} \quad (11)$$

The fractional uncertainty for the charging efficiency is

$$\frac{w_{\eta_{ch}}}{\eta_{ch}} = \left[\left(\frac{w_{Q_{abs}}}{Q_{abs}}\right)^2 + \left(\frac{w_{Q_{str}}}{Q_{str}}\right)^2\right]^{1/2} \quad (12)$$

The fractional uncertainty for the discharging efficiency is

$$\frac{w_{\eta_{disch}}}{\eta_{disch}} = \left[\left(\frac{w_{Q_{str}}}{Q_{str}}\right)^2 + \left(\frac{w_{Q_{use}}}{Q_{use}}\right)^2\right]^{1/2} \quad (13)$$

The studied parameters' fractional uncertainties are tabulated in Table 3.

Table 3 The Studied Parameters Uncertainties

Parameter	Absorbed Power	Discharged Thermal Power	Stored Thermal Power	Charging Efficiency	Discharging Efficiency
Fractional Uncertainty (%)	0.93	0.04	2.8	2.3×10^{-5}	2.2×10^{-5}

3.RESULTS AND DISCUSSION

The results of an experimental work conducted aim to investigate a novel solar air heaters SAH are presented. The new proposed design was a closed SAH system combined with an internal finned heat exchanger filled with phase change material PCM. Fig. 5 depicts the air outlet temperature, PCM temperature, incident solar radiation, and ambient temperature. At the beginning of the experiment, both PCMs' temperatures rapidly increased because the PCMs were in their solid state. During the PCM charging period, the PCM temperature increased as the solar radiation augmented. Within six hours of work (at 2:00 PM), both PCMs reached their maximum temperatures, i.e., 54 °C for RT42 in both connecting arrangements, 59 °C for RT50 in the separation arrangement, and 58 °C in the series arrangement. After 2:00 PM, the PCMs' temperatures dropped with the solar radiation decrease and the ambient temperature increase, so the thermal losses increased. When the discharging started at 5:30 PM, an air blower at 0.065 kg /s through the thermal storage-heat exchanger forced the cold ambient air. At 5:30 PM, both PCMs for both arrangements were at 44 °C. The PCMs' temperatures continued to decrease because the forced air absorbed heat from the PCMs. Besides, the ambient air temperature decreased, leading to increased thermal heat losses. The PCM and the air outlet temperature difference was very low, revealing that the heat exchanged between them was high. The huge heat exchanged between the PCM and the outlet was due to the finned heat exchanger use. At the beginning of the discharging period, the temperature difference was 2 °C for RT42-separation and series arrangements. The RT42 SAH was the first in the series arrangement, and as a result, its behavior was similar to that in the separate arrangement. While for RT50, the temperature difference was 1°C for the separation arrangement and 3 °C for the series arrangement. At the end of the discharging period, the temperature differences were 0.5 °C, 0.7 °C, 0 °C, and 0.1 °C for RT42-separation, RT42-series, RT50-separation, RT50-series, respectively. Fig. 6 shows the stored, discharged, and lost powers during the discharging period for both RT42 and RT50 through solar air heaters at 0.065 kg/s. As the forced air absorbed heat from the PCMs and the thermal losses increased due to ambient temperature drop, the stored power decreased through the discharging period. As the discharging period for RT42 started, the stored power was 1550 W, and the discharged power was 1352 W for both studied arrangements. As the discharging period ended at 3:00 AM, the stored power was 120 W, and the discharged power was 22 W. As for RT50 for the separate arrangement, at the beginning of the discharging period, the stored and discharged powers were 630 W and 535 W, respectively. While at the discharging period end, i.e., at 2:00 AM, the stored and discharged powers were 2.5 W and 5 W, respectively. For the series arrangement, at the beginning of the discharging period, the stored and discharged powers were 12 W and 80 W, respectively. While at the discharging period end, i.e., at 6:00 AM, the stored and discharged powers were 12 W and 0 W, respectively. In other words, the RT50 and the forced air temperature difference was too low to cause heat transfer. From Fig. 6 (a, b), it can be seen that the stored power in RT42 was higher than with RT50. The immense stored power of RT42 resulted from its high latent heat, i.e., 165 kJ/kg K, compared to that of RT50, i.e., 160 kJ/kg K. It can be concluded from Fig. 5 that the discharging of RT42 ended at 3:00 AM in both separation and series arrangements, while RT50 ended at 2:00 AM in the separation arrangement. While at 4:30 AM, the RT42 was completely discharged, so the air inlet temperature applied to the RT50 became similar to the ambient temperature. Therefore, this RT50 discharging continued in the series arrangement to the test end. As the later solar air heater received warm air from RT42 SAH, the configuration with RT50 took more time to discharge. Fig. 7 shows the percentages of the thermal power absorbed by RT42 and RT50 besides the thermal losses from the SAHs during the charging period. Fig. 7 (a, b) assure that the stored power in RT42, i.e., 74%, was higher than that in RT50, i.e., 65%, due to the RT42 high latent heat. The high latent heat of RT42 also decreased RT42 thermal losses compared to RT50 ones. In both RT42 and RT50 SAHs, the heat loss from the glass cover was the highest among other heat losses due to the lack of thermal insulation compared to other SAHs surfaces. Fig. 8 shows that, due to cold weather in winter, the accumulator of the stored power was similar for both paraffin RT42 and RT50 at the beginning of the test, i.e., 8000 kW at 8:00 AM. With ongoing exposure to solar radiation, the wax RT42 reached the phase change region faster than the RT50 due to its lower melting point and large storage capacity. Therefore, the RT42 spent more time in the phase change area; thus, the cumulative stored power of RT50 was higher than with RT42.

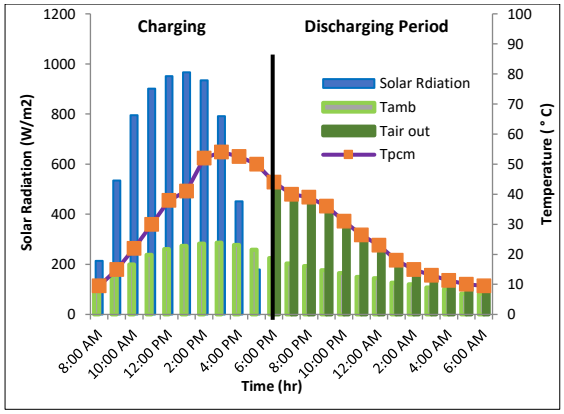

(a)

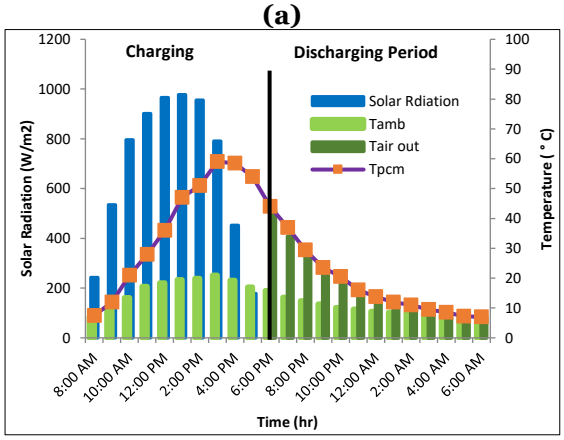

(b)

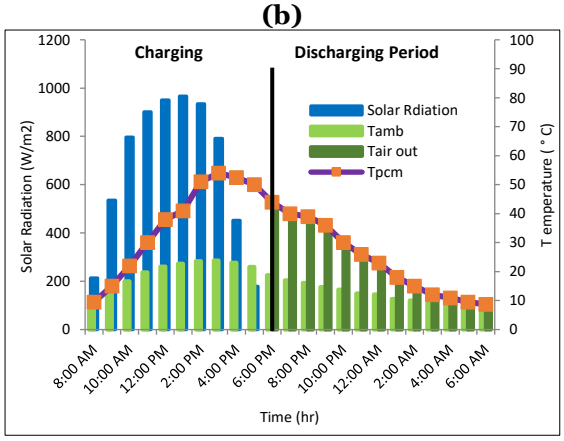

(c)

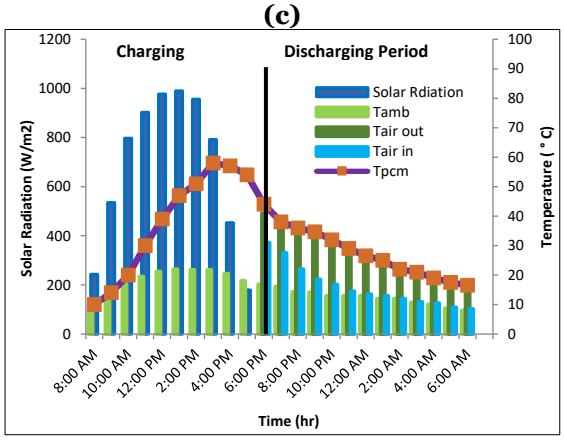

(d)

Fig. 5 Solar Radiation and Temperature Through Experiment Period at 0.065 kg/s for (a) RT42-Separation, (b) RT50-Separation, (c) RT42-Series, and (d) RT50-Series.

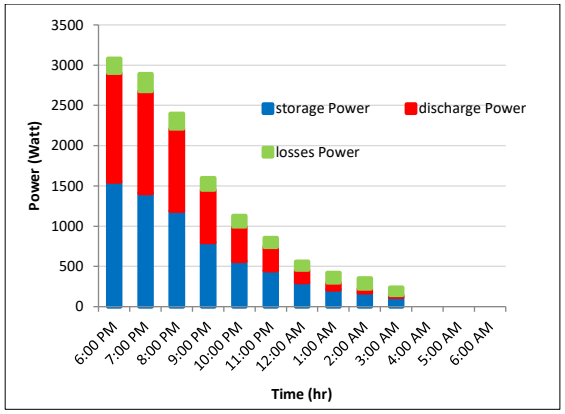

(a)

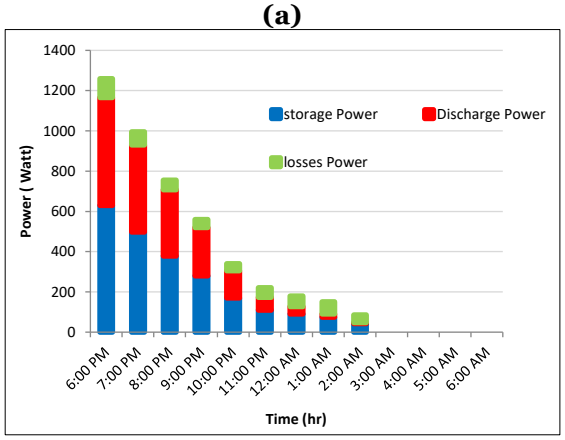

(b)

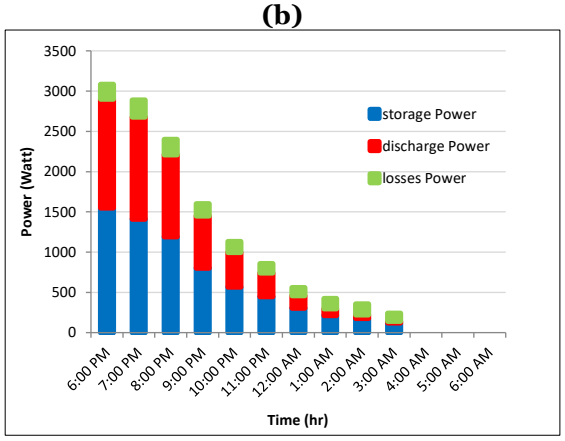

(c)

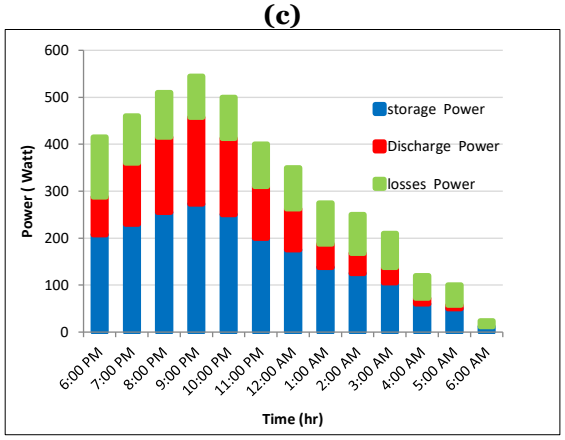

(d)

Fig. 6 Stored, Discharged, and Losses Powers During the Discharging Period at 0.065 kg/s for (a) RT42-Separation, (b) RT50-Separation, (c) RT42-Series, and (d) RT50-Series.

Fig. 9 presents the charging efficiency of both RT42 and RT50 SAHs in separate arrangement during the charging period. As the test began, the charging efficiencies of RT42 and RT50 SAH were 93.1% and 93.2%, respectively. The charging efficiencies were at their highest value at the beginning of the test because the PCMs were in a state of solid, and the absorption rate was at its highest value. With ongoing exposure to solar radiation, the charging efficiency gradually decreased due to increased thermal losses because of the temperature difference augmentation between the PCM and the ambient (Fig.9 (a, b)). The reduction slowed down at noon for both PCMs. From 12:00 PM to 3:00 PM, the average charging efficiency of the RT42 was 73%, and the RT50 was 74%. After 3:00 PM, the charging efficiency significantly dropped due to the solar radiation reduction and the thermal losses increase. As the charging period ended at 5:00 PM, the charging efficiency of the RT42 was 32% and 35.9% for the RT50. Fig. 10 shows the RT42 and RT50 SAHs discharging efficiency in the separation and series arrangements at 0.065 kg/s. The RT42 SAH showed similar behavior in both arrangements since it was the first in the series arrangement. While the SAH with the paraffin RT50 was the second in the series arrangement. The forced air through it was preheated in RT42 SAH configuration. Therefore, the wax RT50 showed a different behavior in the series arrangement. In the case of RT42 in both arrangements and RT50 in the separation arrangement, the discharging efficiency was essential at the beginning of the discharging period, i.e., 85% and 90%, respectively, due to the huge temperature difference between the PCMs and the ambient. With time, the discharging efficiency for the three cases continued to decline due to the decreased stored energy and the increased thermal losses because of the ambient temperature drop. Therefore, the discharging efficiency dropped to zero at 1:30 AM for the RT50-separation case at 2:30 AM for RT42 in both arrangements. As for RT50 in the series arrangement, at the beginning of the discharging period, the discharging efficiency was 20%. The forced air entering the RT50 solar heater in the series case was already preheated in the RT42 solar air heater. Therefore, the temperature difference between the forced air and RT50 was low, reducing the heat transfer rate, which caused a decrease in the discharging efficiency. However, as the ambient temperature kept dropping through the night, the heat transfer rate increased, augmenting the discharging efficiency to reach its highest value of 63% at 10: 00 PM. With ongoing discharging of the stored energy, the discharging efficiency decreased. However, unlike the other three cases, the discharging efficiency of the RT50 solar heater dropped to 15% at the end of the discharging period at 6:00 AM the next day.

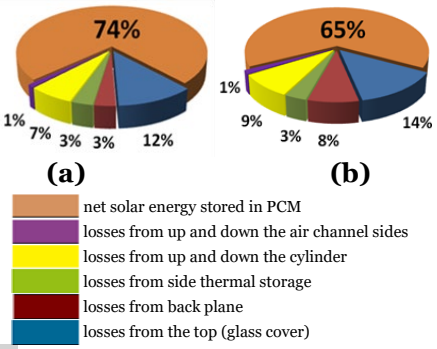

Fig. 7 Percentages of Net Solar Energy Stored in PCM and Thermal Losses from the Solar Air Heaters During the Charging Period (a) RT42, and (b) RT50.

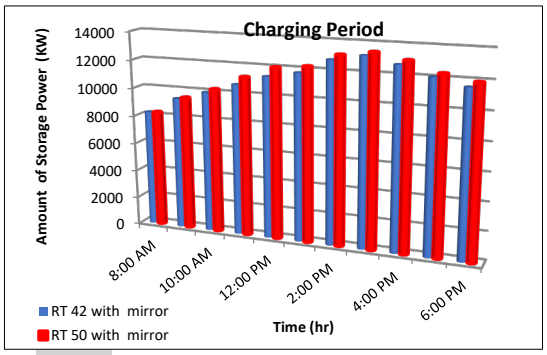

Fig. 8 Stored Powers of RT42 and RT50 During the Charging Period.

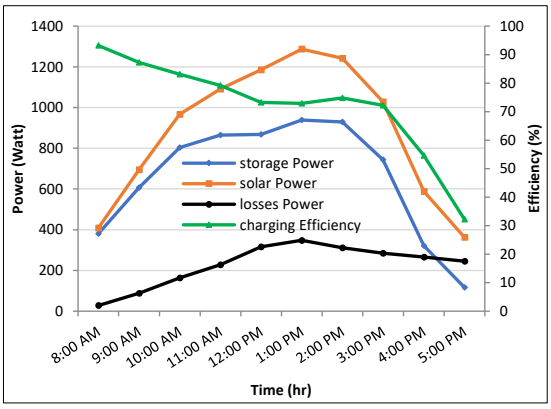

(a)

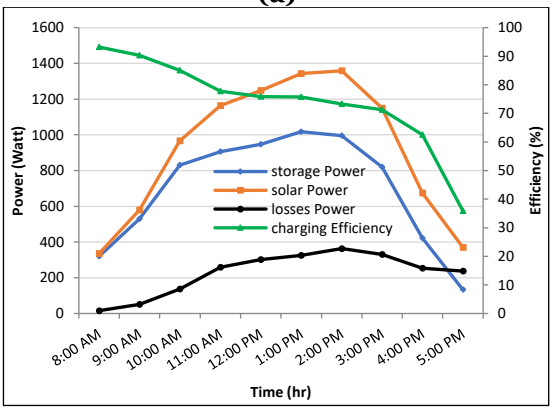

(b)

Fig. 9 The Charging Efficiency of SAHs in the Separate Arrangement (a) RT42 and (b) RT50.

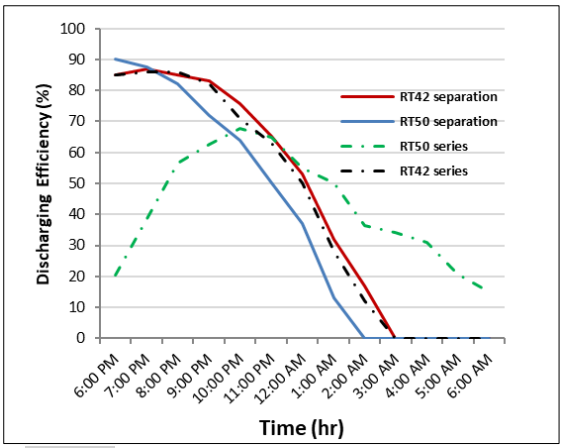

Fig. 10 RT42 and RT50 SAHs Discharging Efficiencies in the Separation and Series Arrangements.

4.CONCLUSIONS

An experimental investigation of a novel SAH design was conducted. The new proposed design was a closed SAH system that included an absorber-thermal storage-finned heat exchanger unit filled with paraffin wax RT42 and RT50. The following are the key obtained conclusions from the experimental results:

- Six hours after starting the experiment (at 2:00 PM), both RT42 and RT50 reached their maximum temperatures. The highest recorded temperature value of RT42 was 54 °C in both connecting arrangements. While with the paraffin RT50, the highest recorded temperature value was 59 °C in the separation arrangement and 58 °C in the series arrangement.
- The discharging period of the RT50 SAH in the series arrangement was extended to 4:30 AM the next day of experiments, and while in the separation arrangement, it ended at 2:00 AM the next day. On the other hand, in the case of RT42, the discharging period ended at 3:00 AM the next day for both arrangements.
- The average charging efficiencies of RT42 and RT50 in mid-day were 73% and 74%, respectively.
- At 6:00 AM the next day, the discharging efficiency of the RT50 solar heater dropped to 15%, contrary to the other three cases that dropped to zero by 3:00 AM.

NOMENCLATURE

Notation	Description
A	Area (m²)
c_p	Specific heat capacity (kJ/kg.°C)
h_f	Latent heat of PCM (J/kg)
I	Incident solar radiation (W/m²)
k	Thermal conductivity (W/m K)
$\dot{m}$	Mass flow rate (kg/s)
P	Power (W)
T	Temperature (°C)
Greek Symbols	
α	Absorptivity
η_{charg}	Charging efficiency (%)
$\eta_{discharg}$	Discharging efficiency (%)
ρ	Density (kg/l)
τ	Transitivity

Subscripts	
abs	Absorber
a-ch	Side air channel
av	Average
b.p	Backplane
c.e	Cylinder ends
g.c	Glass cover
i	Inlet
m	Melting
o	Outlet
s.s.t	Side storage tank

REFERENCES

[1] Kwakwa PA. **The Carbon Dioxide Emissions Effect of Income Growth, Electricity Consumption and Electricity Power Crisis**. *Management of Environmental Quality: An International Journal* 2021; **32**(3):470–487.

[2] Mostafaeipour A, Bidokhti A, Fakhrzad M-B, Sadegheih A, Zare Mehrjerdi Y. **A New Model for the use of Renewable Electricity to Reduce Carbon Dioxide Emissions**. *Energy* 2022; **238**:121602.

[3] Obaideen K, et al. **On the Contribution of Solar Energy to Sustainable Developments Goals: Case Study on Mohammed Bin Rashid Al Maktoum Solar Park**. *International Journal of Thermofluids* 2021; **12**:100123, (1-14).

[4] Abbasi KR, Shahbaz M, Zhang J, Irfan M, Alvarado R. **Analyze the Environmental Sustainability Factors of China: The Role of Fossil Fuel Energy and Renewable Energy**. *Renewable Energy* 2022; **187**:390–402.

[5] Mohammed GA, Mohammed ZS. **Modeling Horizontal Single Axis Solar Tracker Upon Sun-Earth Geometric Relationships**. *Tikrit Journal of Engineering Sciences* 2022; **29**(3):43–48.

[6] Al-Yasiri Q, Szabó M. **Incorporation of Phase Change Materials into Building Envelope for Thermal Comfort and Energy Saving: A Comprehensive Analysis**. *Journal of Building Engineering* 2021; **36**:102122, (1-23).

[7] Huang Y, Liu X. **Charging and Discharging Enhancement of a Vertical Latent Heat Storage Unit by Fractal Tree-Shaped Fins**. *Renewable Energy* 2021; **174**:199–217.

[8] Mlakar U, Zavrl E, Stritih U. **An Experimental and Numerical Analysis of An Improved Thermal Storage Tank with Encapsulated PCM for use in Retrofitted Buildings for Heating**. *Energy and Buildings* 2021; **248**:111196, (1-13).

[9] Jmal I, Baccar M. **Numerical Study of PCM Solidification in A Finned Tube Thermal Storage Including Natural Convection**. *Applied Thermal Engineering* 2015; **84**:320–330.

[10] Jmal I, Baccar M. **Numerical Investigation of PCM Solidification in a Finned Rectangular Heat Exchanger Including Natural Convection**. *International Journal of Heat and Mass Transfer* 2018; **127**:714–727.

[11] Wang T, Diao Y, Zhu T, Zhao Y, Liu J, Wei X. **Thermal Performance of Solar Air Collection-Storage System with Phase Change Material Based on Flat Micro-Heat Pipe Arrays**. *Energy Conversion and Management* 2017; **142**:230–243.

[12] Saxena A, Agarwal N, Cuce E. **Thermal Performance Evaluation of a Solar Air Heater Integrated with Helical Tubes Carrying Phase Change Material**. *Journal of Energy Storage* 2020; **30**:101406.

[13] Kabeel AE, Khalil A, Shalaby SM, Zayed ME. **Experimental Investigation of Thermal Performance of Flat and V-Corrugated Plate Solar Air Heaters with and Without PCM As Thermal Energy Storage**. *Energy Conversion and Management* 2016; **113**:264–272.

[14] El Khadraoui A, Bouadila S, Kooli S, Farhat A, Guizani A. **Thermal Behavior of Indirect Solar Dryer: Nocturnal Usage of Solar Air Collector with PCM**. *Journal of Cleaner Production* 2017; **148**:37–48

[15] Bhowmik H, Amin R. **Efficiency Improvement of Flat Plate Solar Collector using Reflector**. *Energy Reports* 2017; **3**:119–123.

[16] Liu Y, Wang L, Peng L, Zhang S, Lin X, Han X, et al. **Effect of Additives on the Cyclic Thermal Stability and Thermal Properties of Sodium Acetate Trihydrate as a Phase Change Material: An Experimental Study**. *Solar Energy* 2022; **231**:473–483.

[17] Tang X, Xu T, Wang J, Zhang H, Chen J, Huang G, et al. **Preparation and Thermal Properties of a Novel Pseudo Ionic Liquid Phase Change Material for Solar Water Heating System**. *Solar Energy Materials and Solar Cells* 2022; **236**:111507.

[18] Zhou W, Yang Z, Feng Y, Lin L. **Insights into the Thermophysical Properties and Heat Conduction Enhancement of Nacl-Al2O3 Composite Phase Change Material by Molecular Dynamics Simulation**. *International Journal of Heat and Mass Transfer* 2022; **198**:123422.

[19] Senobar H, Aramesh M, Shabani B. **Evacuated Tube Solar Thermal Collector with Enhanced Phase Change Material Thermal Storage: An Experimental Study**. *Journal of Energy Storage* 2022; **46**:103838.

[20] Huang Y, Song L, Wu S, Liu X. **Investigation on the Thermal Performance of a Multi-Tube Finned Latent Heat Thermal Storage Pool**. *Applied Thermal Engineering* 2022; **200**:117658.

[21] Izadi M, Sheremet M, Alshehri HM, Ambreen T, Doranehgard MH. **Numerical Study on Charging Process Inside a Grid-Structure Thermal Storage**. *Journal of Energy Storage* 2022; **45**:103522.

[22] Sajawal M, Rehman T, Ali HM, Sajjad U, Raza A, Bhatti MS. **Experimental Thermal Performance Analysis of Finned Tube-Phase Change Material Based Double Pass Solar Air Heater**. *Case Studies in Thermal Engineering* 2019; **15**:100543, (1-12).

[23] Abuşka M, Şevik S, Kayapunar A. **A Comparative Investigation of the Effect of Honeycomb Core on the Latent Heat Storage with PCM in Solar Air Heater**. *Applied Thermal Engineering* 2019; **148**:684–693.

[24] Dheyab HS, Al-Jethelah MSM, Baccar M. **Closed Collector –Storage Solar Air Heating System Thermal Performance: An Experimental Study**. *Energy Sources, Part A: Recovery, Utilization and Environmental Effects* 2022; **44**(4):10006–10023.

[25] Kalogirou SA. **Solar Energy Engineering: Processes and Systems**. 2nd ed., USA: Academic Press, Elsevier; 2014.

[26] Yassen TA, Mokhlif ND, Eleiwi MA. **Performance Investigation of an Integrated Solar Water Heater with Corrugated Absorber Surface for Domestic use**. *Renewable Energy* 2019; **138**:852–860.

[27] PCM RT-LINE Versatile Organic PCM for Your Application. Rubitherm Technologies GmbH - Imhoffweg 6 - 12307 Berlin. 2022: Available from:https://www.rubitherm.eu/en/productcategory/organische-pcm-rt.

[28] Bhagwat VV, Roy S, Das B, Shah N, Chowdhury A. **Performance of Finned Heat Pipe Assisted Parabolic Trough Solar Collector System under the Climatic Condition of North East India**. *Sustainable Energy Technologies and Assessments* 2021; **45**:101171, (1-49).

[29] Li M-J, Jin B, Ma Z, Yuan F. **Experimental and Numerical Study on the Performance of a New High-Temperature Packed-Bed Thermal Energy Storage System with**

Macroencapsulation of Molten Salt Phase Change Material. *Applied Energy* 2018; **221**:1–15.

[30] Agyenim F. **The use of Enhanced Heat Transfer Phase Change Materials (PCM) To Improve the Coefficient of Performance (COP) of Solar Powered Libr/H 2 O Absorption Cooling Systems**. *Renewable Energy* 2016; **87**:229–239.

[31] Gilago MC, Chandramohan VP. **Performance Evaluation of Natural and Forced Convection Indirect Type Solar Dryers During Drying Ivy Gourd: An Experimental Study**. *Renewable Energy* 2022; **182**:934–945.

[32] Kline SJ, Mcclintock F. **Describing Uncertainties in Single-Sample Experiments**. *Mechanical Engineering* 1953; **75**:3–8.